ACKNOWLEDGMENTS

The authors express their appreciation to Dr. C. T. Candland for his assistance in data analysis and interpretation, and for making several pressure calibration runs relating to the ion-pairing experiment.

†Research supported in part by the National Science Foundation. Based in part on a Ph. D. dissertation submitted to Brigham Young University by H. R. C.

*Present address: Cutter Laboratory, Ogden, Utah.

[1]C. S. Fuller and J. A. Ditzenberger, Phys. Rev. 91, 193 (1953).

[2]C. S. Fuller and J. C. Severiens, Phys. Rev. 96, 21 (1954).

[3]J. R. Haynes and W. Shockley, Phys. Rev. 81, 835 (1951).

[4]H. Reiss, C. S. Fuller, and F. J. Morin, Bell System Tech. J. 35, 535 (1956).

[5]B. Pratt and F. Friedman, J. Appl. Phys. 37, 1893 (1966).

[6]B. I. Boltaks, *Diffusion in Semiconductors* (Academic, New York, 1963).

[7]N. H. Nachtrieb, J. A. Weil, and A. W. Lawson, J. Chem. Phys. 20, 1189 (1952).

[8]N. H. Nachtrieb, H. A. Resing, and S. A. Rice, J. Chem. Phys. 31, 135 (1959).

[9]N. H. Nachtrieb, and A. W. Lawson, J. Chem. Phys. 23, 1193 (1955).

[10]W. C. Dunlap, Jr., Phys. Rev. 94, 1531 (1954).

[11]R. Kubo and T. Nagamiya, *Solid State Physics* (McGraw-Hill, New York, 1969), p. 359.

[12]Reference 4, p. 622.

[13]M. Cardona, W. Paul, and H. Brooks, J. Phys. Chem. Solids 8, 204 (1959).

[14]A. E. Stern and H. Eyring, J. Phys. Chem. 44, 955 (1940).

[15]R. N. Jeffery and D. Lazarus, J. Appl. Phys. 41, 3186 (1970).

[16]J. A. Weyland, D. L. Decker, and H. B. Vanfleet, Phys. Rev. B 4, 4225 (1971).

[17]O. L. Anderson, J. Phys. Chem. Solids 27, 547 (1966).

[18]H. T. Hall, Rev. Sci. Instr. 29, 267 (1958).

[19]H. R. Curtin, D. L. Decker, and H. B. Vanfleet, Phys. Rev. 139, A1552 (1965).

[20]D. L. Decker, Rev. Sci. Instr. 39, 602 (1968).

[21]C. T. Candland, D. L. Decker, and H. B. Vanfleet, Phys. Rev. B 5, 2085 (1972).

[22]R. Glang, J. Electrochem. Soc. 107, 356 (1960).

[23]E. M. Pell, J. Phys. Chem. Solids, 3, 74 (1957).

[24]H. Reiss and C. S. Fuller, J. Phys. Chem. Solids 4, 58 (1958).

[25]C. D. Thurmond and J. D. Struthers, J. Phys. Chem. 57, 831 (1953).

[26]S. N. Vaidya, J. Akella, and G. C. Kennedy, J. Phys. Chem. Solids 30, 1411 (1968).

[27]I. C. Getting and G. C. Kennedy, J. Appl. Phys. 41, 4552 (1970).

[28]R. E. Hanneman, H. M. Strong, and F. P. Bundy, in *Accurate Characterization of the High Pressure Environment*, edited by E. C. Lloyd (National Bureau of Standards, Washington, D. C., 1971).

[29]H. Portnoy, Jr., W. M. Letaw, and L. Slifkin, Bull. Am. Phys. Soc. 30, 13 (1955).

[30]E. Rapoport, J. Chem. Phys. 44, 3581 (1966).

[31]C. A. Wert and C. Zener, Phys. Rev. 76, 1169 (1949).

[32]K. Weiser, Phys. Rev. 126, 1427 (1962).

PHYSICAL REVIEW B VOLUME 5, NUMBER 12 15 JUNE 1972

Trends in the Nearest-Neighbor Distance: Elements and Binary Compounds

Robert W. Shaw, Jr.
Bell Laboratories, Murray Hill, New Jersey 07974
(Received 20 December 1971)

Trends relating nearest-neighbor distance (d) in elemental materials and A^NB^{8-N} compounds to atomic number (Z), valence (z), and principal quantum number (n) of the outermost filled electron shell are reported. These trends can be described by simple functional relationships which are typically accurate to within a few percent. For elements, these relations are $dZ^{1/3}/n \cong$ constant for fixed z, and $d^{1/n}Z \cong \frac{4}{3}(Z - z + 12)$ for fixed n. An analysis of the results based on a Fermi-Thomas model for the core electrons and a free-electron model for the valence electrons is given. The trend observed for the A^NB^{8-N} compounds is that $d\bar{Z}^{1/3}/\bar{n} \cong$ constant for a fixed cation species. This relation is used to construct a modified Mooser-Pearson plot which yields a complete separation of zinc-blende, wurtzite, and rocksalt structures.

I. INTRODUCTION

Crystal structure is perhaps the most fundamental property of a material and at the same time one of the most difficult to understand theoretically. Two rather different approaches have historically been used to discuss crystal structure: (i) the analysis of structural trends in terms of some scaling parameter such as ionicity; and (ii) the detailed computation of the lowest-energy structure

using a first-principles pseudopotential model. The first approach has been widely applied with considerable success by Mooser and Pearson[1] and by Phillips.[2] While structural-trend analysis provides an appealing description of broad classes of materials, it usually fails to provide a precise theoretical description of the structural energy. On the other hand the pseudopotential approach, which was first applied to simple metals by Harrison[3] and has recently been used to discuss a number of metallic systems,[4] has the disadvantage that, for the present, it can be used to investigate only a limited class of materials.

In this paper we shall adopt an approach which is in some ways a combination of both the trend and the pseudopotential analyses. We focus our attention not so much on crystal structure (though we do return to structure at the end) as on the nearest-neighbor distance d. This distance characterizes in a general way the bonding and packing properties of a material and has been the subject of extensive discussion over the years.[5,6] A number of interesting trends[7] have been observed involving the nearest-neighbor distance d, the atomic number Z, the valence z, and the principal quantum number n of the outermost filled shell (referred to as the metallization parameter by Mooser and Pearson[1]). The empirical observations will be presented first and then a simple semiquantitative explanation will be considered for some of the trends in terms of a local-pseudopotential model. At best, however, the success at explaining the observed trends is incomplete and a number of interesting questions which still lack detailed theoretical answers are offered without apology.

Though for clarity in presenting the results of the investigation, we deal first with elemental materials, it is worth noting that trends among the elements were observed only after the corresponding trends in the binary semiconductors and salts had been noticed. This reflects the long-term goal of our study—to understand the origin of complex crystal structures and the relation between structure and the properties of materials. It was in the course of exploring possible extensions of the Phillips theory[2,8] that the author came upon the results to be presented in the present paper.

II. BOND-LENGTH TRENDS AMONG ELEMENTS

We shall direct our attention in this section to the nearest-neighbor distance or shortest bond length d between atoms in their elemental state. When an element occurs with more than one crystal structure we select the shortest nearest-neighbor distance; when it occurs as a molecule, we select the internuclear distance. Our interest will be in studying, and trying to understand, systematic variations of d as a function of the three most fundamental coordinates which characterize the Periodic Table: (a) atomic number Z, (b) column number or valence z, and (c) row number n. If we consider the first full series (Li–F) as row one, then the row number is equivalent to the principal quantum number n of the outermost (highest-energy) filled shell of electrons.

Our initial motivation for considering nearest-neighbor distance was that d enters as an important parameter in the spectral moment approach[8] to calculating ionicity in the $A^N B^{8-N}$ compounds. On further reflection, it becomes clear that d is also a particularly important distance in the elemental materials as well. The majority of elements are found to occur in one of the three structures bcc, fcc, and hcp and for these structures, d is related to the atomic radius by $d \cong 1.8 R_a$, where R_a is defined in terms of the atomic volume Ω by $\Omega = \frac{4}{3}\pi R_a^3$. [We shall use atomic units (a. u.) throughout. In these units, $\hbar = m = c = 1$ and lengths are therefore measured in Bohr radii. Recall that 1 Bohr radius = 0.529 Å.] Hence, for bcc, fcc, and hcp structures, d is a direct measure of atomic volume. For elemental materials occurring in molecular form, d is of course the only relevant distance parameter we have available. When materials occur in distorted structures, e. g., gallium, it is legitimate to ask why d is the relevant distance to consider. A similar question can be asked when we seek to compare materials with metallic structures to those of diamond structure or with materials such as the chalcogenides. To both of these questions we can at present answer only that d appears to exhibit more significant trends than other distance parameters one might consider.

An extensive, entirely empirical, search for trends in d as a function of Z, z, and n has revealed two striking and exceedingly simple relationships which appear to describe trends across the entire Periodic Table with an accuracy which is occasionally 10% and more frequently only a few percent. We shall simply present the data graphically and write down the summarizing relationships in this section, reserving theoretical discussion for Sec. III.

A. Trends for Fixed Valence

The first of these relations is illustrated in Figs. 1–4. We have plotted d/n vs Z on a log-log scale and we find that for each column in the Periodic Table (that is, for fixed valence) the relation

$$dZ^{1/3}/n = f(z) \tag{1a}$$

describes the variation of d. The function $f(z)$ is approximately a constant for fixed z but varies with z as we shall see shortly. Since for the metallic structures (bcc, fcc, hcp) d is proportional to the atomic radius R_a, we can recast (1a) for those

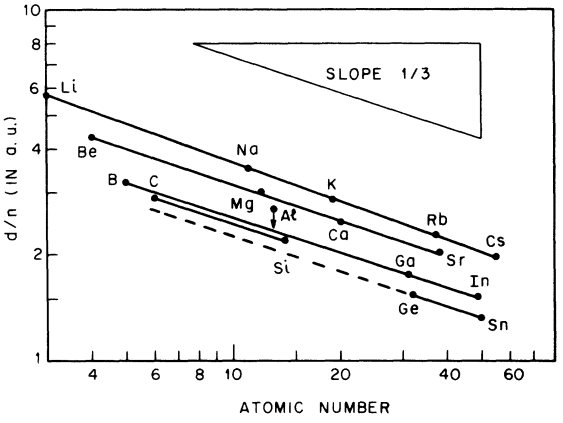

FIG. 1. Nearest-neighbor distance (d) divided by the principal quantum number (n) of the outermost closed electron shell plotted as a function of atomic number for elements of columns IA, IIA, IIIA, and IVA. The arrow indicates that aluminum deviates from the trend appropriate to the other IIIA materials.

structures in the form

$$\Omega Z/n^3 = g(z) \ , \tag{1b}$$

where Ω is the atomic volume and $g(z)$ is a new constant for fixed z. However, (1b) provides a less complete description of the Periodic Table than (1a) since it does not apply to molecular systems or crystals with distorted structures. There are a number of specific comments about the results

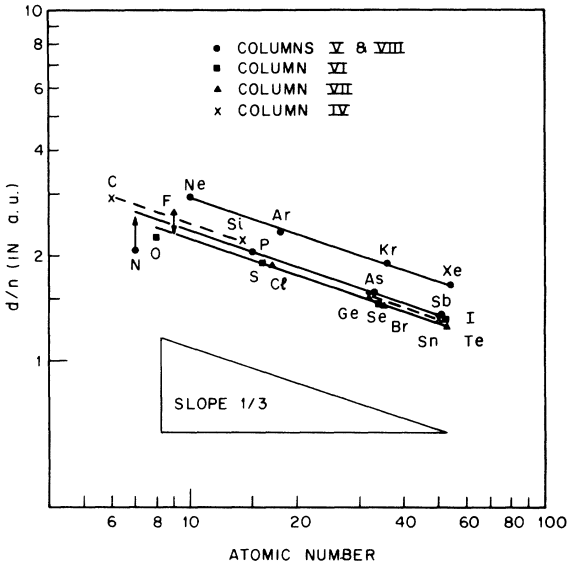

FIG. 2. Log-log plot of d/n vs Z for elements of columns IVA, VA, VIA, and VIIA. As in Fig. 1, arrows indicate significant deviations from over-all trends.

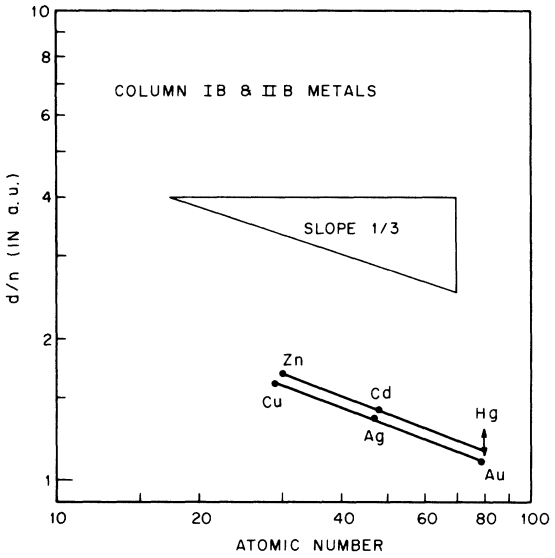

FIG. 3. Log-log plot of d/n vs Z for elements of columns IB and IIB. The arrow here indicates a range of d/n values for Hg.

shown in Figs. 1–4 which are worth making.

(i) By adjusting the slope of the best-fit line around the value $\frac{1}{3}$ it is possible to achieve a more nearly constant $f(z)$.[9] However, the uniform value of $\frac{1}{3}$ for the slope actually yields remarkably constant values of $f(z)$ without requiring any adjustment.

(ii) The fifth-row elements, i. e., Cs–Rn, deviate slightly from the linear relationship (Cs excepted). This is illustrated in Figs. 4 and 5.

(iii) There are several elements which deviate more than a few percent from (1). Aluminum appears to be an open structure relative to the other IIIA elements in that its nearest-neighbor distance is significantly greater than (1) would suggest. It is known, that despite its relatively high electron density, aluminum is the prototypical free-electron metal and seems to have remarkably little covalent character in its bonds.[3] These observations are at least consistent with the apparent openness of its structure. Similarly, fluorine has an anomalously large interatomic distance relative to the other halide molecules. This is consistent with the anomalously large lone-pair weakening of the single bond which is known to occur in the F_2 molecule.[10] On the other hand, nitrogen seems to be more tightly bound in its molecular configuration than (1) would indicate. It is likely that this deviation is associated with the fact that we have used the distance appropriate to the triply-bonded N_2 molecule.

(iv) In the IVA series it appears that two separate values of $f(z)$ provide the best fit, one for C–Si and a slightly different one for Ge–Sn. However, these values are in fact equivalent to within 10%.

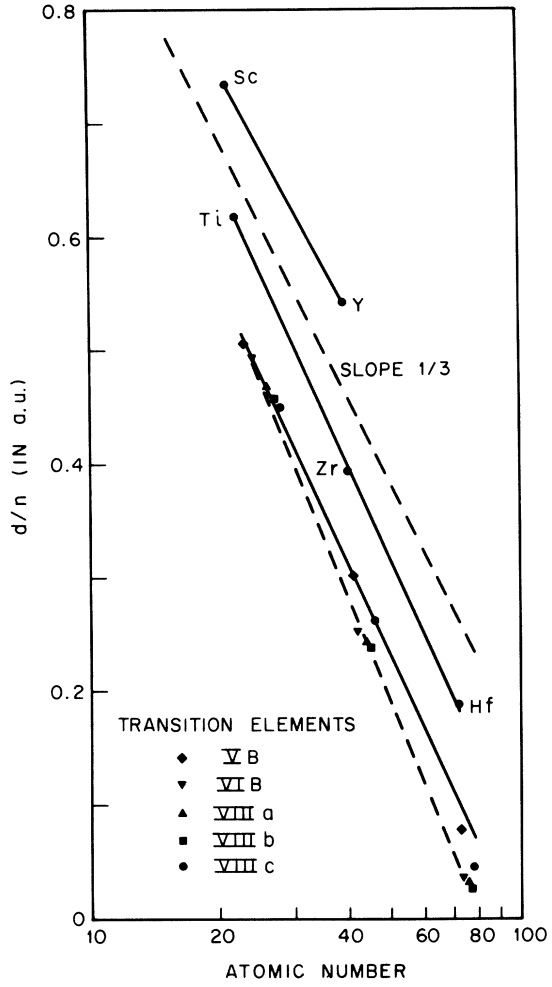

FIG. 4. Log-log plot of d/n vs Z for the transition elements of columns IIIB–VIIIB.

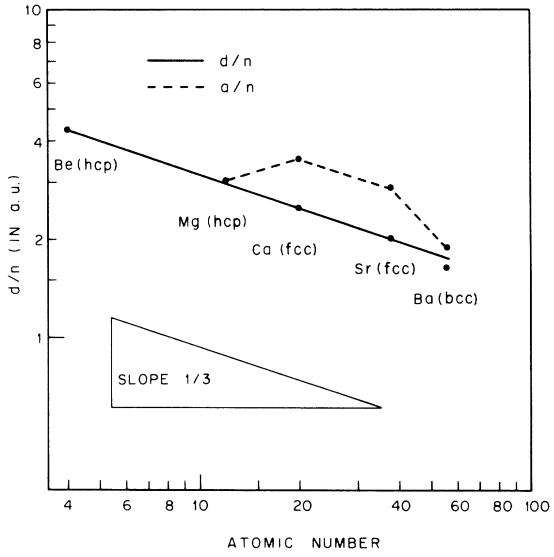

FIG. 5. Trends in nearest-neighbor distance (d) as a function of atomic number compared to similar trends for the lattice parameter (a). Structures of the column IIA elements are indicated. The dashed curve connecting a/n points is intended to illustrate significant deviations from a linear trend.

The question one immediately asks when faced with the results of Figs. 1–4 is whether similar results could be obtained with other combinations of the same parameters. In other words, is Eq. (1) unique to within the prescribed level of accuracy? Our tentative answer would have to be yes. That is to say, that of the numerous simple combinations we have tried, none provides as consistent a description of the data as (1). For example, we indicate in Fig. 5 what one obtains if lattice constants are used in place of nearest-neighbor distance. We have chosen to plot column IIA because of the variety of structures represented. Clearly (1) does not hold if d is replaced by the lattice constant a. This is, of course, not surprising because a is strongly structure dependent, whereas d, as we mentioned earlier, is a measure of atomic volume and consequently provides a more fundamental characterization of the material. As another example, suppose we plot $d/(n+1)$ instead of d/n. The results for column IA, plotted in Fig. 6, are illustrative of the general situation. Apparently only the principal quantum number of the outermost filled shell will do.

The situation for the solid inert "gases" is particularly interesting. We have plotted in Fig. 7 both d/n and $d/(n-1)$ vs Z, where here we think of

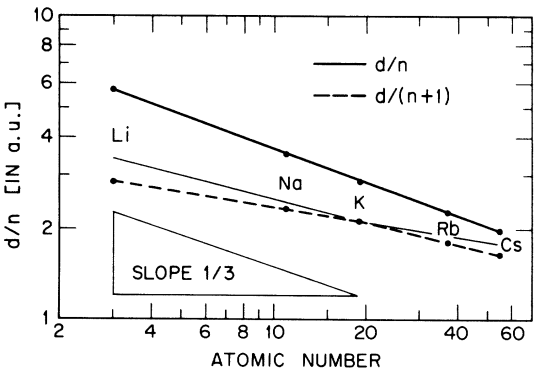

FIG. 6. Illustration that no simple trend is obtained when d, the nearest-neighbor distance, is normalized with the principal quantum number of the valence shell $(n+1)$ rather than that of the outermost closed shell (n). Data for the IA elements are shown. The dashed lines connecting $d/(n+1)$ points (and the extension of these lines) are intended to illustrate the magnitude of deviation from a straight-line trend through all five points.

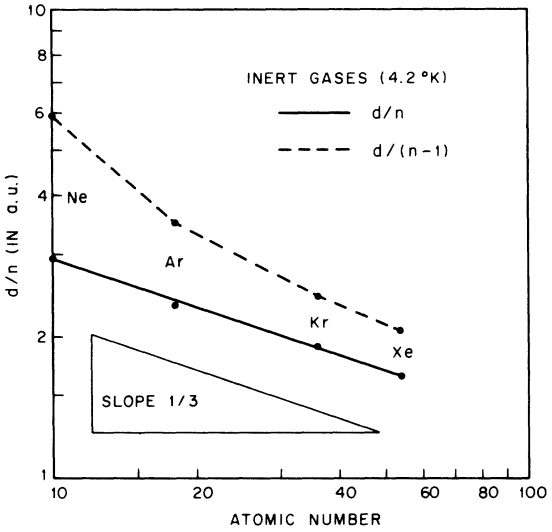

FIG. 7. Log-log plot of d/n vs Z for the "inert-gas" solids; when d is normalized with the principal quantum number of the *outermost* closed shell ($n=2$ for Ne) a linear trend is obtained. If the eight outer electrons are treated as valence electrons ($n=1$ for Ne) then the relation is no longer linear. The dashed line connecting $d/(n-1)$ points is intended to emphasize the deviation from a linear trend.

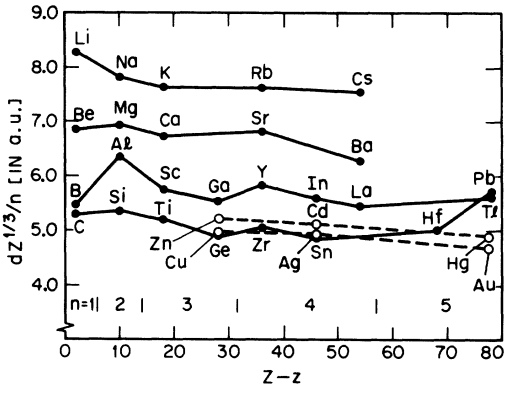

FIG. 8. Function $dZ^{1/3}/n$ vs $Z-z$ for several columns of the Periodic Table. The value of $dZ^{1/3}/n$ is approximately constant for each column. Note that the constant differs for IA and IB columns as well as for IIA and IIB columns, but that the constant is nearly equal for IIIA and IIIB columns.

n only as the quantum number appropriate to the outermost *filled* shell of electrons. It is clear from the figure that it is more consistent with Eq. (1) to think of neon, for example, as the first element in row two with valence 0 rather than the last element in row one with valence 8.

We turn our attention next to the function $f(z)$ which enters Eq. (1). In Fig. 8 we have plotted $dZ^{1/3}/n$ as a function of $Z-z$ for the first four columns of the Periodic Table. In addition to illustrating the approximate constancy of $f(z)$ for fixed z, the figure emphasizes another interesting point, that the constant $f(z)$ for the IB elements is distinctly smaller than that for the IA elements. A similar statement can be made for the IIA and IIB elements. This result is consistent with the usual arguments[4] that the resonant or near-resonant d electrons in the IB and IIB series lead to more closely packed structures than one might expect for mono and divalent metals, based on simple total-energy arguments (see Sec. III).

A more complete illustration of the validity of (1) is given in Fig. 9 where we plot $dZ^{1/3}/n$ vs z. With a very few exceptions, the value of $f(z)$ is constant to within 10% or less for each value of z. The IB and IIB elements appear to have "effective" valences of $z=5$ and $z=4$, respectively, values which agree rather well with those frequently quoted in the chemical literature.[11] The column-VIII elements do not seem to fit the general trend, either as $z=0$ or $z=8$ elements. These exceptions aside, $f(z)$ is a decreasing function of z, obeying a nearly linear relation with approximately integer values for small z and then decreasing less rapidly with increasing z. The quadratic function $f(z) \cong 0.09$

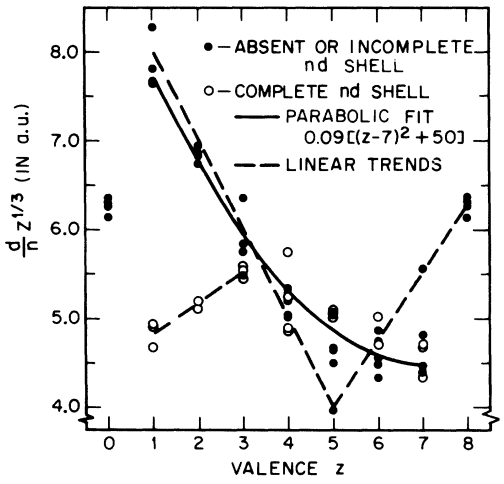

FIG. 9. Function $dZ^{1/3}/n$ vs valence z for all elements in the first four rows of the Periodic Table. For each z the points indicate the spread in values of $f(z)$ [Eq. (1) in text]. A parabolic fit to the basic trend is shown (solid line) and various linear trends are also indicated (dashed lines). The curves shown are only empirical fits to the data and have no detailed theoretical significance. Note that the IB and IIB elements show a distinct deviation from the over-all trend. The "inert-gas" values are plotted both in the $z=0$ and $z=8$ positions and in neither case do they fit the over-all trend.

$\times[(z-7)^2+50]$ is found to give a reasonable empirical fit to the results.

Finally we note that, had we considered trends in atomic radius R_a rather than d, the values of $f(z)$ in Fig. 9 would be reduced by a factor of approximately 1.8 for $z=0$, 1, 2, 3, by 1.4 for $z=4$, and by somewhat smaller factors for the remaining crystalline materials. (R_a is not well defined for molecules so we would have to omit elements occurring in the molecular state from the discussion.) The net effect would be to produce a sharp knee in the $f(z)$ function at $z=4$ with $f(z)\cong$ constant for elements with $z\geq 4$.

B. Trends for Fixed Row Number

Before discussing the above results in detail, we go on to consider the second of the general trends we have observed. In Fig. 10 we plot $d^{1/n}Z$ as a function of z for fixed n, and note immediately a remarkable regularity in the results. Within each row of the Periodic Table, the value of $d^{1/n}Z$ appears to be constant to within a few percent, though a gradual rise with increasing z is discernible. For

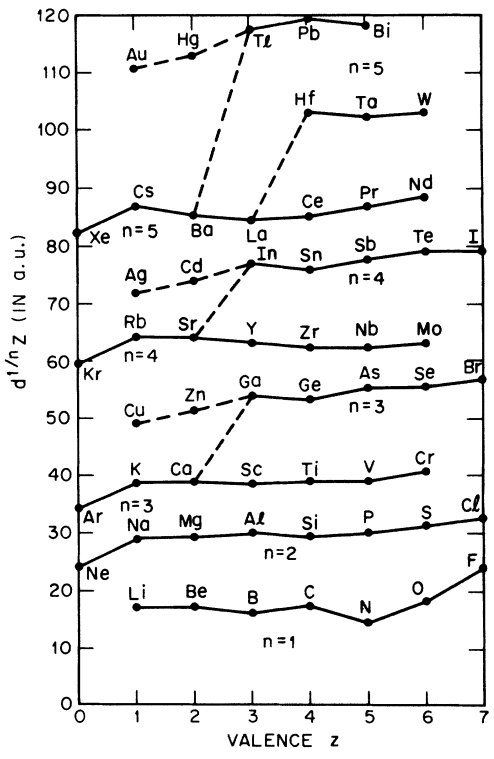

FIG. 10. Values of $d^{1/n}Z$ as a function of valence for elements from the first five rows of the Periodic Table. For a fixed value of n, the function $d^{1/n}Z$ is essentially constant for each distinct value of Z-z within the row.

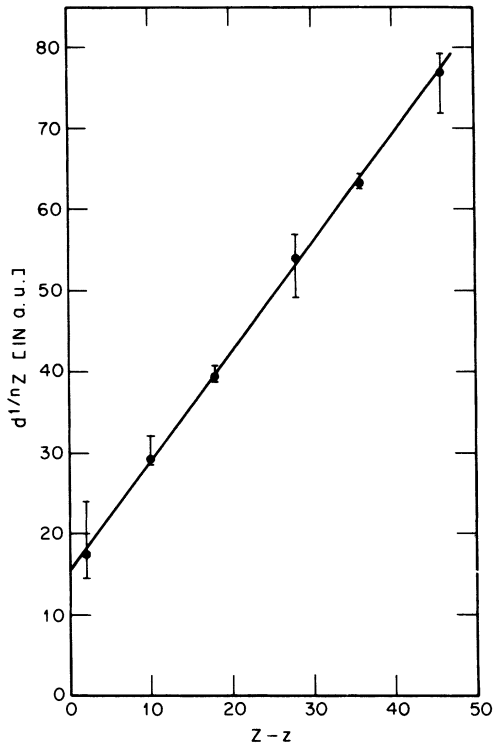

FIG. 11. Function of $d^{1/n}Z$ vs $Z-z$. The error bars indicate the spread of values obtained for elements in each row. The point is the mean value for all elements in the row. A linear fit to the points is shown and represents the result given in Eq. (2) of the text.

$n=3$, 4, 5 there is a distinct constant for those elements with filled d or f shells. The constant values of $d^{1/n}Z$ are found to scale linearly with Z-z as we show in Fig. 11. Slight deviations from the linear fit arise when we reach values of Z-z appropriate to row five and the lanthanide series. However, we should note that even for the heavy elements, $d^{1/n}Z$ is approximately constant for fixed n.

The linear relation illustrated in Fig. 11 can be represented analytically as

$$d^{1/n}Z\cong\tfrac{4}{3}[(Z-z)+12]\ . \qquad (2)$$

Nitrogen and fluorine of the first-row elements deviate from (2) by as much as 20%. Deviations throughout the next five rows of the Periodic Table are less than ten percent and typically only a few percent. Equation (2), then, is a remarkable general result which describes, with considerable accuracy, trends in the nearest-neighbor distance throughout the Periodic Table.

III. THEORETICAL DISCUSSION

The two relations we have obtained in Sec. II involve the same physical parameters and describe

trends in nearest-neighbor distance when valence z and row number n are held constant, respectively. One might suggest that a single relation should describe both trends since, in effect, Eqs. (1) and (2) define grid lines on a log-log plot of d/n vs Z. Such a relation would describe a surface, or surfaces, in the four-dimensional $[d, n, z, Z]$ space, and the equations we have given would be the projections for fixed z and n. There are two possibilities which can be explored immediately.

First, we might attempt to eliminate one of the variables from the two equations, either directly (which does not yield a particularly appealing result) or by developing a third relation between the variables. An immediate candidate for the latter approach would be a relation between the principal quantum number n and $(Z - z)$. We show in Fig. 12 a plot of n^2 vs $(Z - z)$ which indicates an approximate linear relation of the form $n^2 \cong 0.4(Z - z)$. This expression averages the ten-electron spread occurring in rows three and four. Unfortunately we find that if we use this expression to replace n in (1) and (2), the results exhibit less consistent trends and, consequently, we have not pursued this approach further.

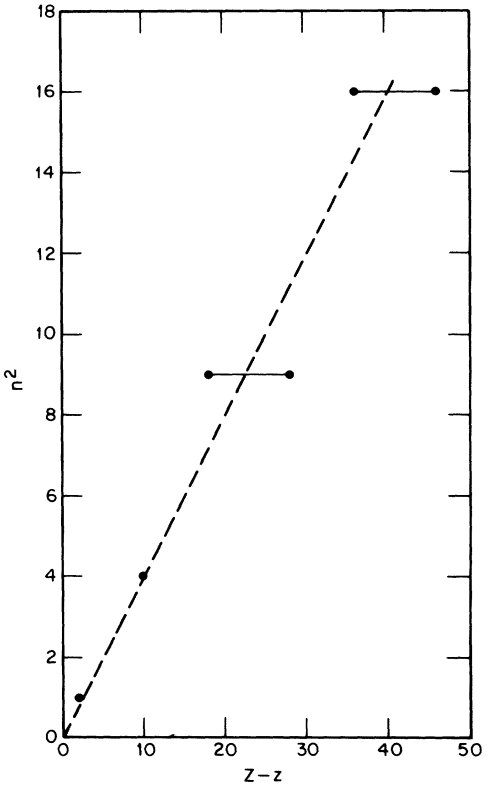

FIG. 12. Plot of n^2, where n is the principal quantum number of the outermost closed electron shell, vs the number of core electrons $(Z - z)$ for elements in the first four rows of the Periodic Table. The two values for $n = 3$, 4 correspond to elements with unfilled and filled outer d shells, respectively.

The second approach is to consider d/n as the first term in an expansion of some function such as $(1 + d)^{1/n}$ and identify this second function in an approximate way with $d^{1/n}$. We have explored a number of possibilities along these lines without notable success. It is interesting to note that d/n and $d^{1/n}$ bear a resemblance to arithmetic and geometric means. While suggestive, this observation has not led to a detailed theoretical connection between (1) and (2). Essentially then, we must leave open the question of a unifying expression and address ourselves to each expression separately.

We have made the most progress in understanding Eq. (1), and hence will proceed now with a brief theoretical analysis. The presence of a $Z^{1/3}$ factor in (1) suggests immediately the Fermi-Thomas statistical model[12,13] and we shall pursue this approach.

The derivation of the Fermi-Thomas equation is given in many texts,[14] and need not be repeated here. The idea is to assume that, within a small region of space around the nucleus of an atom, the potential $V(r)$ varies sufficiently slowly that it may be treated as a constant. Within this region we then treat the Z atomic electrons (core plus valence) as a degenerate electron gas with "local" Fermi-momentum $k_F(r) = [-2V(r)]^{1/2}$. The local electron density is then (in atomic units throughout)

$$n(r) = [-2V(r)]^{3/2}/3\pi^2 \ , \tag{3}$$

and we use this expression in the Poisson equation to obtain a self-consistent equation for the potential

$$\frac{d^2\theta(x)}{dx^2} = \frac{\theta^{3/2}(x)}{x^{1/2}} \ . \tag{4}$$

This is the Fermi-Thomas equation in dimensionless form with $\theta(x) = -rV(r)/Z$ and $x = 4(2/9\pi^2)^{1/3} r Z^{1/3}$. We may now take the "free-atom" boundary conditions $\theta(0) = 1$ and $\theta(\infty) = 0$ and solve (4) by machine. Calculations of this sort have been carried out by a number of authors,[15-18] and we have repeated them only for later computational convenience.

Alternatively we might consider using the "metallic" boundary condition $\theta'(x_c) = \theta(x_c)/x_c$ in place of the "atomic" condition $\theta(\infty) = 0$. However, to determine the cell radius x_c it is necessary to specify the energy zero in some consistent, but arbitrary, way, whereas in the atomic case we can set this constant equal to zero. We have therefore considered only the atomic case in detail.

We begin by computing the dimensionless radius x_0 inside of which all but the z valence electrons are contained. It is straightforward to show that

this radius is defined by the condition

$$\theta(x_0) - x_0\theta'(x_0) = z/Z \quad . \tag{5}$$

We may think of $r_0 = 0.885x_0/Z^{1/3}$ as equivalent to the "core" or model radius R_M which would enter in the local approximation to the optimized model potential,[19,20] and we shall *assume* that r_0 does not change from the atomic value as we form a molecule or a solid.

We have solved (5) numerically for z/Z ratios appropriate to elements in the first four rows of the Periodic Table and have plotted the resulting x_0 as a function of $Z^{1/3}$ in Fig. 13. It is an empirical fact that for each column in the Periodic Table, the results are described almost exactly by a straight line. Furthermore, all the lines have nearly identical ($Z = 0$) intercepts which leads us to the interesting result that

$$r_0 \cong 6.5(1/z^{1/3} - 1/Z^{1/3}) \tag{6}$$

is the general solution of (5) with precision approaching computational accuracy. In other words, the Fermi-Thomas model leads empirically to a simple analytic form (6) for the "core" radius.

A similar approach would be to determine the radius at which the Fermi-Thomas potential intersects the Coulomb potential. This corresponds to the condition $\theta(\tilde{x}_0) = z/Z$ and here the radius $\tilde{r}_0 = 0.885\tilde{x}_0/Z^{1/3}$ would be the appropriate radius to use in the so-called "empty-core" pseudopotential.[4,21] If we solve for $\tilde{x}_0$, we again find that $\tilde{x}_0$ is linear in $Z^{1/3}$ for each column in the Periodic Table but we do not obtain a simple relation such as (6) for $\tilde{r}_0$. Consequently we have not explored this case in detail.

We return, then, to the result (6) for the model-potential core radius r_0 and plot in Fig. 14 the computed values of $2r_0$ as a function of the experimental nearest-neighbor distance. We include in this figure all elements in the first four rows of the Periodic Table except those from columns IB and IIB, which we exclude because, as observed earlier, the neighbor distances are significantly reduced by resonance or near-resonance d-electron bonding. It is clear from Fig. 14 that there is a nearly linear relation between r_0 and d:

$$d \cong 2(1 + r_0). \tag{7}$$

The "inert-gas" solids follow a similar, though shifted, linear relation.

Equation (7) implies a very simple explanation for the nearest-neighbor distance in an elemental solid or molecule, namely, that d is the sum of atomic "core" radii r_0 plus a distance of about 2 a. u. determined by the valence electrons. Of course (7) is only approximately correct but it suggests that we consider a model in which we imagine Fermi-Thomas cores immersed in a free-electron gas of density $n = 3z/4\pi R_a^3$, where R_a is the atomic

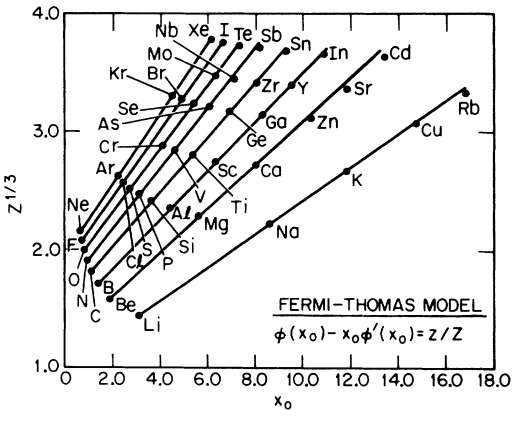

FIG. 13. Dimensionless core radii x_0 calculated from the Fermi-Thomas model [Eq. (5) of the text] shown plotted as a function of $Z^{1/3}$ for elements in the first four rows of the Periodic Table. The linear interpolations satisfy Eq. (6) of the text.

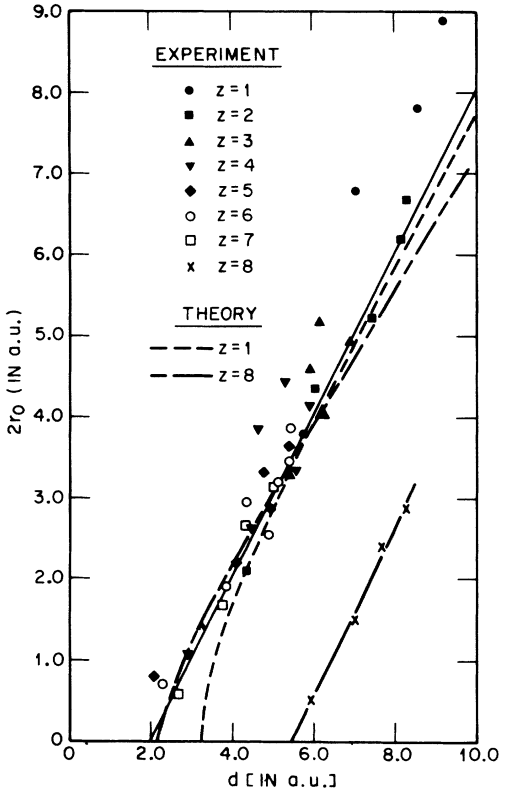

FIG. 14. Plot of calculated Fermi-Thomas core radii r_0, determined by Eq. (5) of the text, as a function of the observed nearest-neighbor distance d for elements from the first four rows of the Periodic Table. The theoretical curves are obtained from Eq. (10) of the text and the linear fit is described by Eq. (7). The inert gases follow a displaced linear relation.

radius introduced earlier.

We pursue this free-electron model a bit further and consider a simple expression for the total energy of a solid.[4,22] Let the potential of an ion have the local-optimized-model-potential form[19,20]

$$V(r)=\begin{cases}-Z/R_M, & r<R_M\\ -Z/r, & r>R_M\end{cases} \tag{8}$$

and set $R_M=r_0$ as determined from the Fermi-Thomas model. Then we write the total energy as (the reader is referred to the review article by Heine and Weaire[4] for details)

$$U=\frac{1.105z^{5/3}}{R_a^2}-\frac{0.458z^{4/3}}{R_a}-\frac{0.9z^2}{R_a}+\frac{z^2}{2R_a}\left(\frac{r_0}{R_a}\right)^2 . \tag{9}$$

The first term in (9) is the kinetic energy of the valence electrons, the second is their exchange energy, the third term arises from the structure-independent part of the Ewald electrostatic energy, and the last term is the contribution from the model potential. We have ignored all structural contributions to the energy as well as the correlation energy of the valence electrons, all of which are small contributions relative to the terms we have included. If we minimize (9) with respect to R_a we obtain an equilibrium cell radius and hence a nearest-neighbor distance, $d\cong 2R_a$, of the form

$$d=\frac{2.21z^{1/3}}{(0.9z^{2/3}+0.458)}\times\{1+[1+0.31(2r_0)^2(0.9z^{2/3}+0.458)]^{1/2}\} . \tag{10}$$

[Precisely speaking, $d/R_a=1.76$ (bcc), 1.81 (fcc), 1.81 (hcp), and 1.40 (diamond). For distorted structures, other values are appropriate. Our use of a uniform value $d/R_a=2$ for all structures therefore introduces some error.]

This result is plotted in Fig. 14 for $z=1$ and $z=8$ and we see that it provides a reasonable description of the data, though certainly no more accurate a description than the simple linear fit given by (7). If we substitute (6) for r_0 in (7) we obtain immediately the proportionality between d and $Z^{-1/3}$. This proportionality also follows from (10) in the large-Z limit. We should emphasize, however, that the above discussion does not give any explanation for the appearance of the quantum number n in the empirical relation (1). Recently Van Vechten and Phillips[6] have discussed the radii of covalently bonded elements in terms of a modified Slater[5] treatment in which the core radius is proportional to n^2 divided by an effective atomic number. However, this approach does not lead to the linear dependence of d on n which we have observed. The combination of Eqs. (1) and (7) suggests that the core radius r_0 might be determined by the sum of n equally spaced shells. However, such a model is certainly not compatible with detailed quantum calculations of core charge densities for the elements.

It remains to provide a detailed quantum treatment which will explain the appearance of n in (1) and, perhaps more important, the remarkably precise empirical expression given in Eq. (2). We have considered a perturbative solution of a one-electron Hamiltonian in the small-(z/Z) limit without any notable success. Possibly the trends we have described are too gross to be amenable to detailed theoretical explanation, but that would be contrary to one's expectation that simple general results can be understood in a reasonably straightforward way. For the moment, however, we must leave our puzzle largely unresolved.

IV. TRENDS AMONG A^NB^{8-N} COMPOUNDS

Our investigation of lattice-constant trends began with the observation that the lattice parameters of the A^NB^{8-N} salts and semiconductors exhibit systematic behavior. This seemed an important observation since the lattice parameter (or nearest-neighbor distance[8]) is an important scaling parameter used to determine the homopolar energy gap in the Phillips theory of ionicity and crystal structure in the A^NB^{8-N} compounds.[2] Evidently trends in lattice parameter, or in d, might bear some relation to trends in crystal structure and we set out initially to explore this possibility.

Note that for the A^NB^{8-N} materials it makes little difference whether we consider trends in the nearest-neighbor distance d or in the lattice constant a. This is because for a fixed cation species the A^NB^{8-N} compounds are isostructural. The one exception to this rule is the sequence MgO–MgTe in which a change from rocksalt to wurtzite structure occurs. We have found that the magnesium compounds can be included in our trend analysis if we work with d rather than a, and for this reason alone the results which follow are given in terms of d.

Motivated by the work of Mooser and Pearson,[1] we introduce an average "metallization" parameter $\bar{n}$ which is the average of the row numbers for the A and B constituents, $\bar{n}=\frac{1}{2}(n_A+n_B)$. We then note that the trends in the distance d of closest approach of the two species in an A^NB^{8-N} compound can be summarized by the relation

$$d\bar{Z}^{1/3}/\bar{n}=A_c , \tag{11}$$

where $\bar{Z}=\frac{1}{2}(Z_A+Z_B)$ is the average atomic number and A_c is a constant for fixed cation (c) species. This relation is exactly analogous to Eq. (1) given earlier for the elements. We illustrate Eq. (11) in Figs. 15–17 and in Table I we have listed the

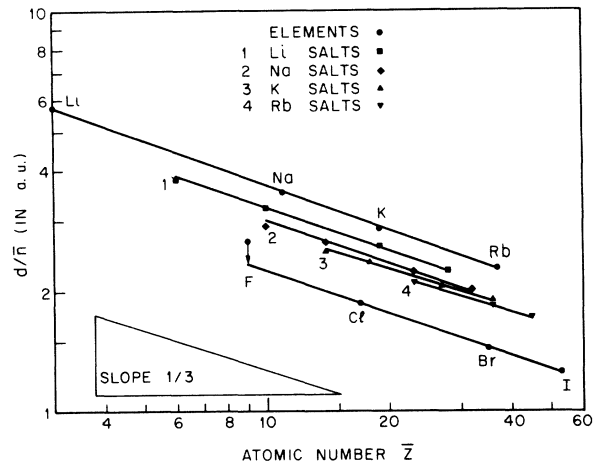

FIG. 15. Log-log plot of $d/\bar{n}$ vs $\bar{Z}$ for the alkali-halide salts ($A^N B^{8-N}$, $N=1$) with $\bar{n}=\frac{1}{2}(n_A+n_B)$ and $\bar{Z}=\frac{1}{2}(Z_A+Z_B)$. The linear behavior is described by Eq. (11) of the text. Values of d/n vs Z for the elemental constituents are shown for comparison.

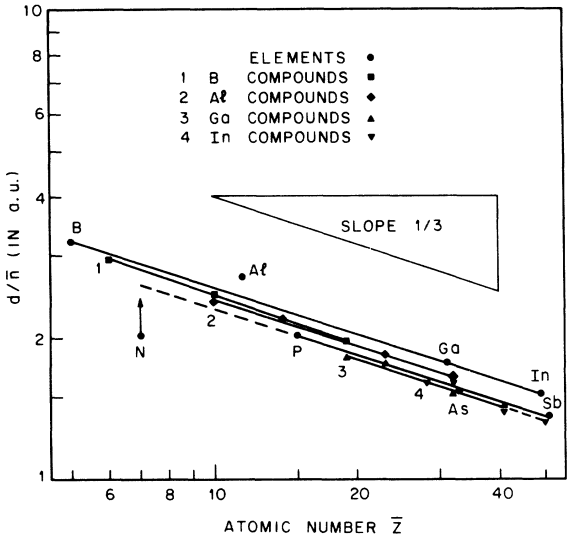

FIG. 17. Log-log plot of $d/\bar{n}$ vs $\bar{Z}$ for the $A^N B^{8-N}$ compounds of $N=3$. The linear behavior is described by Eq. (11) of the text. The values of d/n vs Z for the elemental constituents are shown for comparison.

values of A_c for the alkali halides in order to show that (11) is valid to within a few percent.

There are several additional points of interest to note: (a) While Eq. (11) holds for a fixed cation, a similar relation does not seem to exist for a fixed anion, as is clear from Table I. (b) The value of A_c shows a general tendency to decrease with increasing cation row number, though there are exceptions to this trend. For example, A_c is lower for the Be salts than for the Mg salts. (c) The values of A_c always fall between the corresponding $f(z)$ for the constitutent elements. Roughly speaking, if we linearly interpolate between the appropriate $f(z)$ values on Fig. 9 we can read off A_c at $z=4$. However, this method does not lead to a very accurate determination of A_c. (d) The compound BSb cannot be prepared, perhaps because B has a slightly greater electronegativity than Sb. If BSb could be formed we would expect it to have the zinc-blende structure with a nearest-neighbor distance of $d \cong 4.3$ a. u.

At present we can offer no particularly convincing theoretical explanation for Eq. (11). For one thing, it is not clear why the result is specific to a fixed cation species. For another, it is difficult to understand why the average quantities $\bar{n}$ and $\bar{Z}$ enter as they do. In particular, from the Fermi-Thomas approach discussed in Sec. III we might anticipate an averaging of the core radii $\bar{r}_0 \sim 1/Z_A^{1/3} + 1/Z_B^{1/3}$ to enter. However, if we introduce averages of this sort we find no systematic trends. This may be due to the large energy differences in

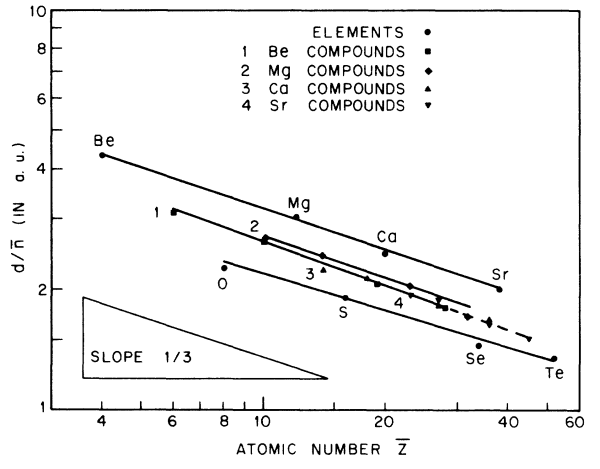

FIG. 16. Log-log plot of $d/\bar{n}$ vs $\bar{Z}$ for the $A^N B^{8-N}$ salts and semiconductors of $N=2$. The linear behavior is described by Eq. (11) of the text. Values of d/n vs Z for the elemental constituents are shown for comparison.

TABLE I. Values of A_c [Eq. (11)] are given for the alkali halides. The values of $f(z)$ for the constituent elements are included for reference.

	Halides	F	Cl	I	Br
Alkalis	$f(z)$	5.57	4.83	4.72	4.73
Li	8.28	6.90	6.96	6.94	6.89
Na	7.81	6.27	6.44	6.39	6.47
K	7.64	6.09	6.23	6.24	6.30
Rb	7.64	6.06	6.22	6.11	6.17

the Fermi-Thomas potential $V(r_0)$ at the "core" radii of the A and B constituents. Evidently the equilibrium distance is determined by an energy minimization which leads to rather different averaging of the critical parameters than we might at first expect. Finally it is important to note that we do not observe for the $A^N B^{8-N}$ compounds any trend analogous to Eq. (2) for the elements, a fact which may reflect only that we do not have any theoretical guideline to motivate a selection of the appropriate parameters.

Having observed a trend in the lattice parameters of the $A^N B^{8-N}$ compounds, we consider next the possibility of using this trend to classify the structures assumed by these materials. We construct a modified Mooser-Pearson plot,[1] replacing their "metallization" parameter $\bar{n}$ by the parameter $\bar{Z}/\bar{n}^3$ which is proportional to the inverse cube of the nearest-neighbor distance, and hence approximately related to Phillips's homopolar energy gap[2] for a particular material. In Fig. 18, we give a plot of $\bar{Z}/\bar{n}^3$ against the electronegativity difference $\Delta X = X_B - X_A$ for the $A^N B^{8-N}$ compounds and we observe immediately a separation of the plot into three regions corresponding to each of the three structures assumed by these materials. The plot is more dramatic than Phillips's plot[2] in that it separates not only covalent and ionic structures but the intermediate wurtzite structures as well. However, it has the disadvantage that the boundaries between the regions do not as yet have a well-defined theoretical interpretation, a disadvantage shared by the Mooser-Pearson plots.[1]

Our motivation for constructing Fig. 18 was not so much to give another two-coordinate plot separating the $A^N B^{8-N}$ materials by structure, but to look for a scheme which could be used to understand structural differences in other classes of materials in terms of simple combinations of fundamental parameters rather than having to rely on a detailed theory which may be relevant to only one type of material. As an example, we have constructed a plot such as Fig. 18 for the several score materials assuming one of the three Laves intermetallic phases.[23] While the resulting plot does not yield the precise separation found in Fig. 18, it does reveal some interesting trends, but that is the subject for another paper.

V. SUMMARY

To conclude briefly, we have presented several simple expressions which describe, with remarkable accuracy, trends in the nearest-neighbor distance of both elements and the $A^N B^{8-N}$ compounds as a function of atomic number, valence, and the principal quantum number of the outermost closed shell of electrons. The key equations which summarize these empirical results are (1), (2), and (11). In addition, we have provided some discussion of the results and a brief theoretical analysis of Eq. (1) in terms of a Fermi-Thomas model for the atomic radii and a free-electron model for the valence electrons. We have also remarked on the numerous puzzling questions which have arisen from these observations and which await detailed theoretical interpretation.

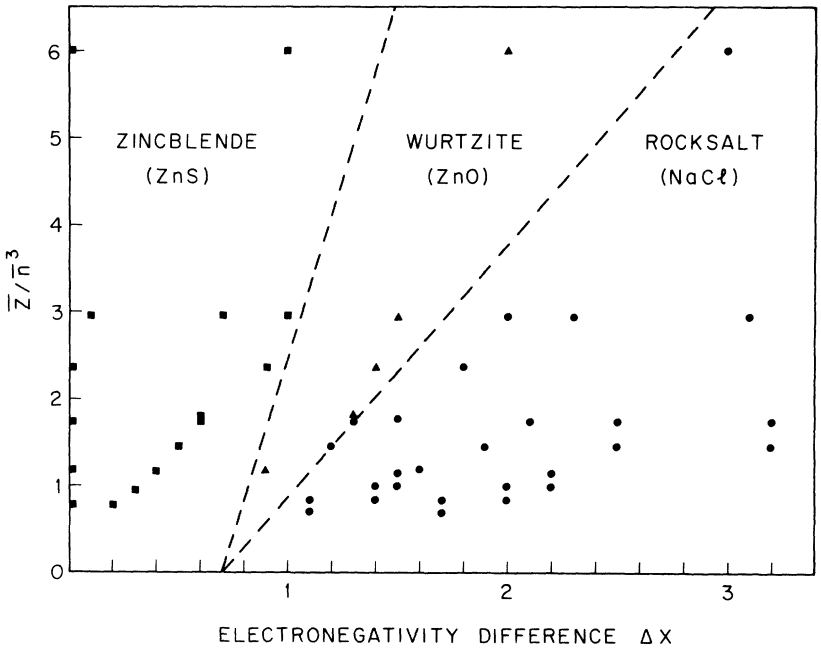

FIG. 18. Modified Mooser-Pearson plot for the $A^N B^{8-N}$ compounds. The ordinate is the average atomic number divided by the cube of the average row number and is proportional to the inverse cube of the nearest-neighbor distance. The abscissa is the Pauling electronegativity difference $\Delta X = X_B - X_A$. The dashed lines separate materials with the three basic structures zinc blende, wurtzite, and rocksalt, but otherwise have no theoretical significance. The materials on the wurtzite-rocksalt boundary are MgS and MgSe, which assume both structures.

ACKNOWLEDGMENTS

Helpful comments from P. W. Anderson, J. C. Phillips, D. B. McWhan, and J. H. Wernick are gratefully acknowledged.

[1]E. Mooser and W. B. Pearson, Acta Cryst. 12, 1015 (1959).

[2]J. C. Phillips, Rev. Mod. Phys. 42, 317 (1970).

[3]W. A. Harrison, Phys. Rev. 129, 2512 (1963); *Pseudopotentials in the Theory of Metals* (Benjamin, New York, 1966).

[4]For a review, see V. Heine and D. Weaire, in *Solid State Physics*, edited by H. Ehrenreich (Academic, New York, 1970), Vol. 24.

[5]J. C. Slater, Phys. Rev. 36, 57 (1930); *Quantum Theory of Molecules and Solids* (McGraw-Hill, New York, 1965), Vol. 2.

[6]J. A. Van Vechten and J. C. Phillips, Phys. Rev. B 2, 2160 (1970).

[7]After this work had been completed it was found that some of the trends noted here were discussed by Hume-Rothery (Ref. 9) in an early paper which seems not to be widely known. However, the present analysis is sufficiently distinct and self-contained that it complements and extends Hume-Rothery's earlier work.

[8]R. W. Shaw, Jr., Phys. Rev. Letters 12, 818 (1970).

[9]W. Hume-Rothery, Phil. Mag. 10, 217 (1930).

[10]R. T. Sanderson, *Chemical Bonds and Bond Energy* (Academic, New York, 1971).

[11]See, for example, C. A. Coulson, *Valence* (Oxford U.P., Oxford, 1961), p. 341.

[12]L. H. Thomas, Proc. Cambridge Phil. Soc. 23, 542 (1927).

[13]E. Fermi, Z. Physik 48, 73 (1928).

[14]See, for example, L. Schiff, *Quantum Mechanics* (McGraw-Hill, New York, 1955), Vol. 2, p. 281; and L. Knopoff, in *High Pressure Physics and Chemistry*, edited by R. S. Bradley (Academic, New York, 1965), Chap. 5.

[15]V. Bush and S. H. C ldwell, Phys. Rev. 38, 1898 (1931).

[16]J. C. Slater and H. M. Krutter, Phys. Rev. 47, 559 (1935).

[17]R. Latter, J. Chem. Phys. 24, 280 (1956); Phys. Rev. 99, 510 (1955).

[18]N. H. March, Proc. Cambridge Phil. Soc. 48, 665 (1952).

[19]R. W. Shaw, Jr., Phys. Rev. 174, 769 (1968).

[20]R. W. Shaw, Jr., Phys. Rev. B 5, 4742 (1972).

[21]N. W. Ashcroft, Phys. Letters 23, 48 (1966).

[22]N. W. Ashcroft and D. C. Langreth, Phys. Rev. 155, 682 (1967).

[23]For a review and references, see J. H. Wernick, in *Intermetallic Compounds*, edited by J. H. Westbrook (Wiley, New York, 1967), Chap. 12, p. 197.

PHYSICAL REVIEW B VOLUME 5, NUMBER 12 15 JUNE 1972

Lowest-Order Optical Nonlinearity in InSb: Theory of Dispersion near the Band Gap

Sudhanshu S. Jha* and James J. Wynne

IBM Thomas J. Watson Research Center, Yorktown Heights, New York 10598

(Received 6 March 1972)

A model for the lowest-order optical nonlinearity in InSb is presented. A method for ensuring the cancellation of sizeable contributions throughout the Brillouin zone is incorporated in the model. A calculation, based on the band structure of InSb at $k=0$, successfully accounts for the dispersion of the optical nonlinearity near the band gap, measured by a second-harmonic-generation (SHG) experiment in InSb. General results are also presented on the interpretation of SHG measurements in absorbing media, with special attention devoted to interference experiments. From a comparison of the experimental dispersion with the theory, values are obtained for momentum matrix elements near $k=0$.

I. INTRODUCTION

The recent measurements by one of us[1] (JJW), of second-harmonic generation (SHG) in InSb, revealed a surprisingly large frequency dependence of the nonlinear susceptibility $\chi^{(2)}(-2\omega, \omega, \omega) = \chi^{(2)}(\omega+\omega)$ near the band gap. In addition, the magnitude of $\chi^{(2)}(\omega+\omega)$ was found to be significantly larger than the calculated static values.[2,3] No experimental measurements of the static value for InSb exist. We have examined the possible contributions to the dispersion observed by JJW and have developed a model based on the band structure of InSb at $k=0$. This model successfully accounts for the experimental results. In calculating $\chi^{(2)}$ from the band structure, we recognize the need to ensure the cancellation of sizeable contributions throughout the Brillouin zone. This cancellation is automatic when the exact band structure is used. But an approximate band structure can lead to noncancellation unless further